17th World Conference on Earthquake Engineering, 17WCEE
Sendai, Japan - September 13th to 18th 2020

SHAKING TABLE TESTS ON CHINESE STYLE SUSPENDED CEILING SYSTEMS

H.J. Jiang[(1)], Y. Wang[(2)], K. Kasai[(3)], S. Motoyui[(4)], T. Chhat[(5)]

[(1)] *Professor, International Joint Research Laboratory of Earthquake Engineering, Tongji University, Shanghai 200092, China, jhj73@tongji.edu.cn*
[(2)] *PHD candidate, International Joint Research Laboratory of Earthquake Engineering, Tongji University, Shanghai 200092, China, yongwang0305@163.com*
[(3)] *Professor, Institute of Innovative Research, Tokyo Institute of Technology, Yokohama, Kanagawa 226-8503, Japan, kasai.k.ac@m.titech.ac.jp*
[(4)] *Professor, School of Environment and Society, Tokyo Institute of Technology, Yokohama, Kanagawa 226-8502, Japan, motoyui.s.aa@m.titech.ac.jp*
[(5)] *Master candidate, Graduate School of Environment and Society, Tokyo Institute of Technology, Yokohama, Kanagawa 226-8502, Japan, chhat.t.aa@m.titech.ac.jp*

Abstract

The failure of suspended ceiling systems (SCSs) has been one of the most widely reported seismic damage to non-structural components (NSCs) in buildings in recent years. To examine the seismic performance of Chinese style SCSs, the full-scale shaking table tests on Chinese style SCSs installed on a steel platform were conducted. Two specimens with the same plane dimensions of 12.52mx5.32m, one denoted as Ceiling A without seismic clips and the other denoted as Ceiling B with seismic clips, were constructed and tested in order to compare the failure modes, dynamic properties and responses including acceleration, displacement and strain responses. Several sets of input motions were selected, including sweep waves varying in frequency from 5.0Hz to 0.5Hz or 0.8Hz in order to explore the failure mechanism of the ceiling and acceleration responses at different floors of a 128-story super-tall building structure benchmark model and a 30-story stick model obtained by time history analysis. The tested ceiling exhibited the damage modes similar to those found in the real earthquake. The failure of SCS was mainly caused by the high vulnerability of peripheral components and grid connections. The boundary of SCS in weak axis direction, which is perpendicular to main tees, is the weak part of SCS. The natural frequencies of the two ceilings were obtained by using the transfer function method. The natural frequencies of Ceiling A extremely affected by the pounding at the boundary are larger than those of Ceiling B. It is found from the test results that the seismic performance of the ceiling is significantly affected by the boundary condition. With the installation of seismic clips at the boundary, the responses of ceilings, such as acceleration, displacement and strain, decrease significantly, and the collapse resistance capacity is improved.

Keywords: Non-structural components, suspended ceiling systems, shaking table tests, seismic performance

1. Introduction

During moderate or major earthquakes in recent years the damage to non-structural components (NSCs) led to great property loss, interruption of building function and even threat to life safety although the main building structures suffered minor damage [1-8]. As one of the most popular NSCs in buildings, the suspended ceiling systems (SCSs) suffered serious damage. The common types of damage to SCSs include dislodgement and falling of ceiling panels, unseating of ceiling grid members around the perimeter, buckling and failure of ceiling grid connections, buckling of ceiling grid members, failure of supporting elements, failure of ceiling connectors and collapse of ceilings [9, 10].

To examine the seismic behaviour and vulnerability of SCSs and enhance the seismic performance of SCSs during earthquakes, experimental and fragility studies mainly utilizing shaking table tests have been carried out for nearly fourty years since the early 1980s [11-22]. Although some valuable conclusions have been drawn from previous experiments, such as the measures including pop rivets and seismic clips could significantly improve the seismic performance of SCSs, they applied only to the cases of low to mid-rise buildings. The seismic behaviour of SCSs in super-tall buildings could be different from those in shorter buildings. It is necessary to investigate the performance of SCSs under the long period vibration loading condition of super-tall buildings. As the experience during the 2011 Tohoku earthquake showed that a major subduction earthquake occurring at a considerable distance away can precipitate long duration ground shaking motion in the city of Tokyo. The super-tall buildings in Tokyo with distance of 400km from the epicenter during the 2011 Tohoku earthquake did not suffer any structural damage, while the loss of super-tall building function from the coupling effects of long period and long duration earthquake motions resulted in a large number of evacuees and business interruption [23, 24]. Therefore, it is necessary to evaluate the seismic performance of SCSs under this type of excitation.

Despite the wide application of NSCs in China, it was not until the 2013 Lushan earthquake that the failure of NSCs, including SCSs, attracted considerable attention from Chinese researchers [21]. Recognizing that SCSs are extremely vulnerable to earthquake, several shaking table tests of SCSs have been conducted to investigate the seismic performance of SCSs [21, 22]. Wang et al. [21] performed shaking table tests on a SCS with the plane dimensions of 3.1mx3.7m installed on a full-scale single-story RC frame to study the damage mechanism of SCS. The tests partially reproduced the observed damage of SCSs in the real earthquake. In the study by Lu et al. [22], the shaking table tests on three types of SCSs with different supporting structures and construction details installed on a 3-story steel frame were conducted to mitigate the seismic damage to SCSs in large-span spatial structures. The experimental results indicated that the supporting flexible structure could increase the vertical response of the suspended ceiling and the vertical response of the ceiling decreased to a certain extent when a hinge was included in the hanger rod in the middle.

Although seismic clips are recommended by Chinese standard J502-2 [25], no relevant investigation has been carried out on the effect of seismic clips on the seismic performance of Chinese style SCSs. Previous earthquake damage [26] indicated that the SCS without seismic clips was highly prone to continuous collapse due to the gird members near the ceiling perimeter easily falling off from the wall angles during earthquakes. Although good seismic performance of the US-style ceiling with seismic clips was proved by some researchers [27, 28], the Chinese style ceiling is quite different from the US-style ceiling, such as: (1) threaded rods rather than hanging wires are more popularly adopted to hang the grid system, resulting in the difference of load-resisting path between them; (2) carrying channels are widely used in the Chinese style ceiling, resulting in the ceiling being double layer rather than single layer. Therefore, the seismic performance of Chinese style ceilings with seismic clips needs to be verified by shaking table tests.

To address the above shortcomings, the shaking table tests on the full-scale Chinese style SCSs installed on a steel platform were carried out in this study to achieve a better understanding of the response characteristics and seismic behaviour of Chinese style SCSs with seismic clips. Two specimens with seismic clips or not were strictly designed and constructed according to Chinese standard J502-2 [25], JGJ339 [29]

and CECS255 [30]. In the paper the detailed description of the test program was firstly presented, and then experimental results such as the failure process, dynamic characteristics, acceleration, displacement and strain responses were analyzed.

2. Test program

2.1 Test setup

The shaking table test is the most common method of evaluating the seismic performance of SCSs. The steel platform was used as a test carrier to hang the ceiling. The design of the platform should take into account two basic requirements: (a) the platform has a high fundamental frequency outside of the range of natural frequencies of suspended ceilings to avoid resonance; (b) the platform has reasonable height to facilitate ceiling assembly, maximize its rigidity and minimize the need of calibration of the excitations input to the specimens. Based on the above considerations, the steel platform was designed and constructed for the full-scale shaking table test on Chinese style SCSs. It has two-story with the plane dimensions of 12.84mx11.64m and the height of 5.40m, as shown in Fig. 1.

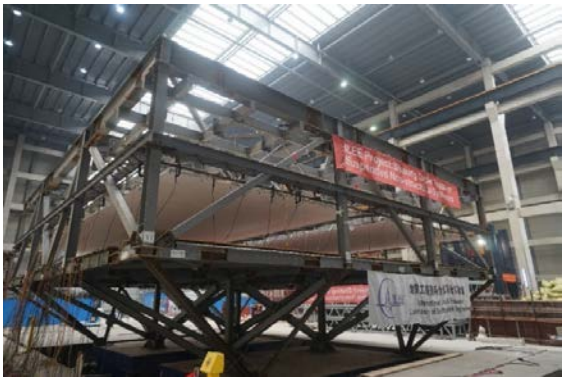

Fig. 1 – Overall view of the steel platform

2.2 Test specimens

The SCS tested here is one type of Chinese SCSs widely used in public buildings in China, with exposed grids and acoustic lay-in panels, easily leveled and constructed due to the existence of carrying channels. It is comprised of load-carrying channels, a grid system, threaded rods, lay-in panels and accessories. The load-carrying channel generally refers to U-section one mainly used to increase the vertical stiffness and facilitate levelling the ceiling. A grid system consists of main tees, cross tees forming a module for placing lay-in panels. Threaded rods are the load-bearing members of hanging a grid system and lay-in panels from the bottom of the supporting floor slab. The typical ceiling accessories include hangers attaching threaded rods to U-section carrying channels, hooks connecting U-section carrying channels and main tees, screws fastening wall angles to the wall, and seismic clips constraining the peripheral grids to the wall angles.

To more intuitively compare the seismic performance of the Chinese style SCSs with seismic clips or not, two specimens with the same area of 12.52mx5.32m were suspended from the bottom of the same floor to ensure the same input excitation. Two specimens were identical except the boundary condition. The plan layout of specimens is shown in Fig. 2a. The specimen without seismic clips was denoted as Ceiling A, and the other with seismic clips is denoted as Ceiling B. In Ceiling A all peripheral grid ends were free and just sitting on the wall angles installed on the board with screws, as shown in Fig. 2b. In Ceiling B seismic clips were installed at the peripheral grid ends on the boundary, as shown in the Fig. 2c. Besides, the peripheral main tees and cross tees were fixed to the wall angles at the north and west sides (N-W sides) while the peripheral grid ends at the south and east sides (S-E sides) were designed as free sliding bearings only along the axis of the ceiling grids.

Unlike the US-style ceiling with a grid system directly hung by hanger wires, the Chinese style ceiling consisted of two-layer grid system (Fig. 2d), which was suspended via the threaded rods with the diameter of 8mm and the length of 1000mm under the top steel beams. Threaded rods were placed at 1200mm intervals. The carrying channel was attached to the threaded rod by the hanger through a bolt and three nuts, and then the hook with a matched hole allowing 3600mm long main tee to pass through was connected to the carrying channel. Main tees were placed parallel to each other at intervals of 1200mm along the Y direction. Cross tees had two different lengths of 1200mm and 600mm. The 1200mm-long cross tees were placed perpendicular to main tees, and the 600mm-long cross tees were used parallel to the main tees. Interlocking main tees and cross tees through mechanical connections formed a grid system, providing a module for lay-in panels simply resting on the flange of each tee, whose nominal dimension is 600mmx600mm squares with a thickness of 16mm. Wall angles fixed to the board on the boundary supplied vertical support for the grid system.

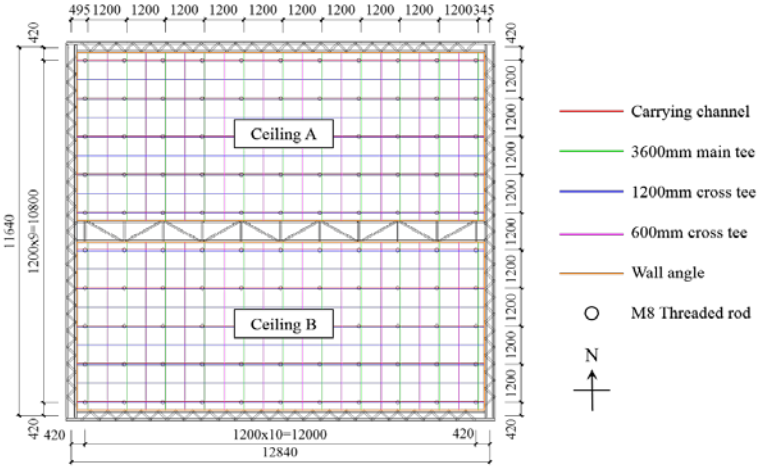

(a) Plan layout of test specimens

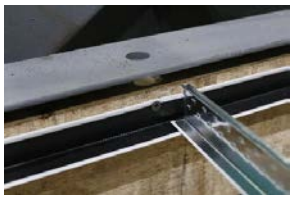

(b) Ceiling A

(c) Ceiling B

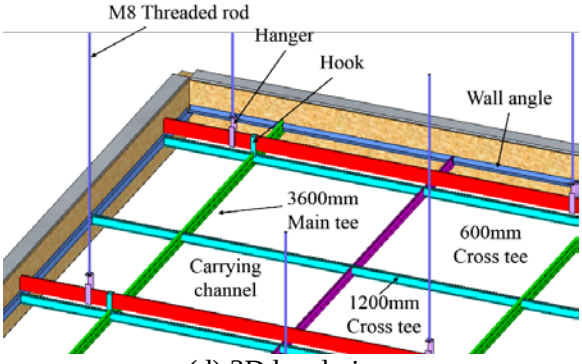

(d) 3D local view

Fig. 2 – Overall view of test specimen

2.3 Instrumentations

The location and number of accelerometers installed on the platform are shown in Fig. 3a. To verify the real input of the shaking tables, one 3-axes accelerometers were placed on the shaking tables. There were 5 and 4 accelerometers installed on the top floor (UF level) and peripheral beams (PB level), respectively.

A total of 210 instruments including 30 accelerometers, 40 displacement transducers and 140 strain gauges were installed on the specimens to measure the respones of the ceiling system. The location and number of these instruments are shown in Fig. 3b.

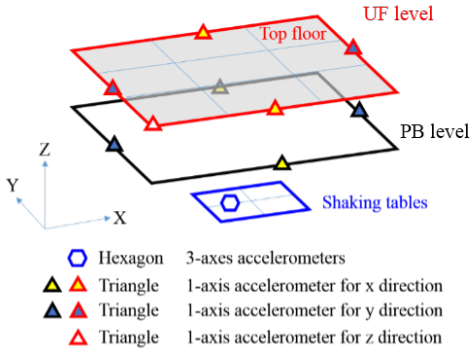

(a) Accelerometers on the steel platform

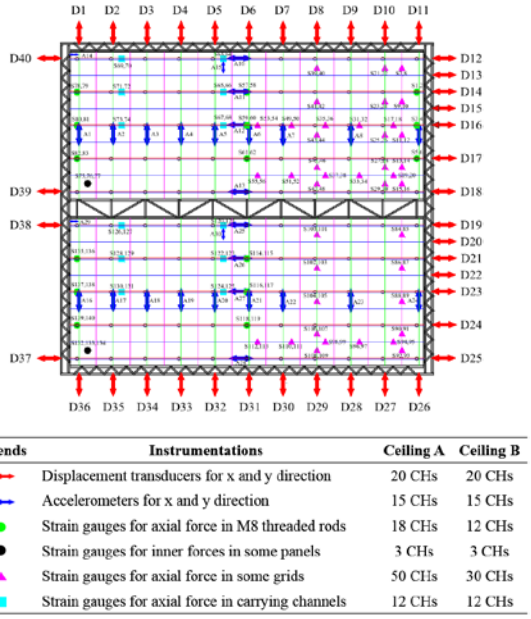

Legends	Instrumentations	Ceiling A	Ceiling B
	Displacement transducers for x and y direction	20 CHs	20 CHs
	Accelerometers for x and y direction	15 CHs	15 CHs
	Strain gauges for axial force in M8 threaded rods	18 CHs	12 CHs
	Strain gauges for inner forces in some panels	3 CHs	3 CHs
	Strain gauges for axial force in some grids	50 CHs	30 CHs
	Strain gauges for axial force in carrying channels	12 CHs	12 CHs

(b) Instruments on the ceiling

Fig. 3 – Instruments on test specimens

2.4 Load protocol

Several sets of motions were carefully selected and input to the table, including sweep waves varying in frequency from 5.0Hz to 0.5Hz or 0.8Hz to explore the failure mechanism of the ceiling, acceleration responses at different floors of super-tall building structures obtained by time history analysis, and artificial wave created by the Building Center of Japan (named as BCJ-L2). One of the sweep wave is shown in Fig. 4.

The natural seismic wave (named as SHW6) with the predominant period of 0.9s was selected, which is specified in Shanghai seismic design code [31]. The basic earthquake with the PGA of 100gal was considered as base input to the analytical models, with the exceeding probability of 10% in 50 years in Shanghai. The acceleration responses at different floors of 128-story Benchmark model and 30-story stick model were derived by time history analysis. The 128-story Benchmark model was established based on the prototype of Shanghai Tower by using software PERFROM-3D [32]. The natural vibration periods of the first three modes were 8.94s, 8.93s and 4.48s, respectively. The acceleration responses at the 5th and 128th floor of the model were used as input motions here. The natural vibration periods of the first three modes of the 30-story stick model were 3.01s, 1.18s and 0.72s, respectively. The acceleration responses at the top were used as input motions. Table 1 lists all the input motions for the test. For all the singular runs bi-direction white noise with a PGA of 50gal was input.

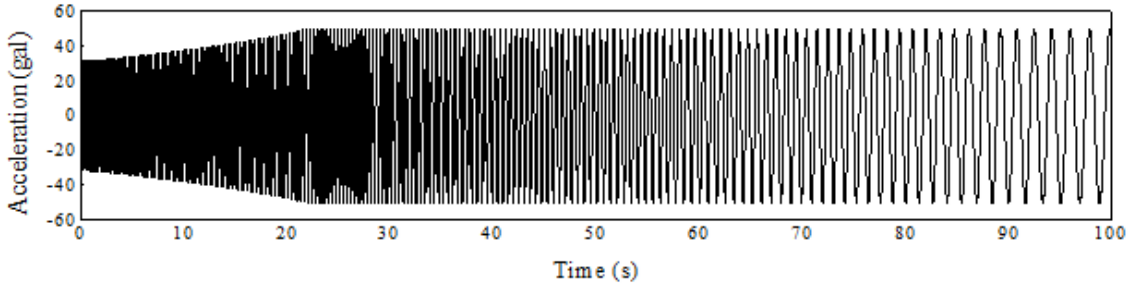

Fig. 4 –Sweep wave

Table 1 – Details of input excitations

Run no.	Input motion	PGA (gal) X dir.	PGA (gal) Y dir.	Duration (s)	Note
2	Sweep	50	0	100	f=5.0～0.5Hz
4	Sweep	0	50	100	f=5.0～0.5Hz
6	BCJ-L2	37	0	120	Ground motion
8	BCJ-L2	0	37	120	Ground motion
10	SHW6-5-story	89	70	70	Resp. at 5th floor of 128-story benchmark model
12	SHW6-128-story	149	132	70	Resp. at 128th floor of 128-story benchmark model
14	SHW6-30-story	405	377	150	Resp. at the top of 30-story stick model
16	Sweep	150	0	100	f=5.0～0.5Hz
18	Sweep	0	150	100	f=5.0～0.5Hz
20	Sweep	250	0	100	f=5.0～0.5Hz
22	Sweep	0	250	100	f=5.0～0.5Hz
24	Sweep	500	0	100	f=5.0～0.8Hz

3. Test results

3.1 Failure process

The observed failure process of two specimens is summarized in Table 2 and Fig. 5 showing the sequence of damage to the components of SCS. The damage to the two ceilings after the last run was shown in Fig. 6. After the input of sweep wave with the highest intensity in X direction the rapid unseating of peripheral grid ends from the wall angles, the huge pounding between the ceiling edge and surrounding board, the failure of a large number of ceiling grid connections, and the subsequent falling of lay-in panels supported on grids occurred in Ceiling A, whereas no panels falling off and only a few grid connections buckling and failing were observed in Ceiling B. Compared with Ceiling B, the ratio of falling lay-in panels to total panels reached 71.03% for Ceiling A after all runs were completed. Compared with Ceiling A, the damage to Ceiling B was much slighter. The above results reveal that the Chinese style SCS with seismic clips has better seismic performance than the one without seismic clips.

Table 2 – Failure process of ceiling specimens

Serial no.	Damage mode	Ceiling A	Ceiling B
1	Unseating of grid	Y	N
2	Buckling of wall angle	Y	N
3	Buckling of grid connections	Y	Y
4	Sliding of hook	Y	Y
5	Dislodged panel	Y	Y
6	Failure of grid connections	Y	Y
7	Falling of panel	Y	N
8	Buckling of grid	Y	N
9	Failure of hanger and hook	Y	N
10	Falling of grid	Y	N
11	Complete collapse	Y	N

Note: Y and N refers to Yes and No, respectively.

(a) Unseating of grid

(b) Buckling of wall angle

(c) Buckling of grid connections

(d) Sliding of hook

(e) Dislodged panel

(f) Failure of grid connections

(g) Falling of panel

(h) Buckling of grid

(i) Failure of hanger and hook

(j) Falling of grid

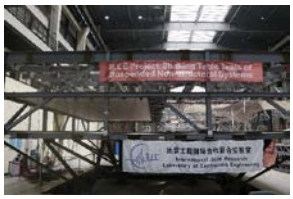

(k) Complete collapse

Fig. 5 – Failure process during test

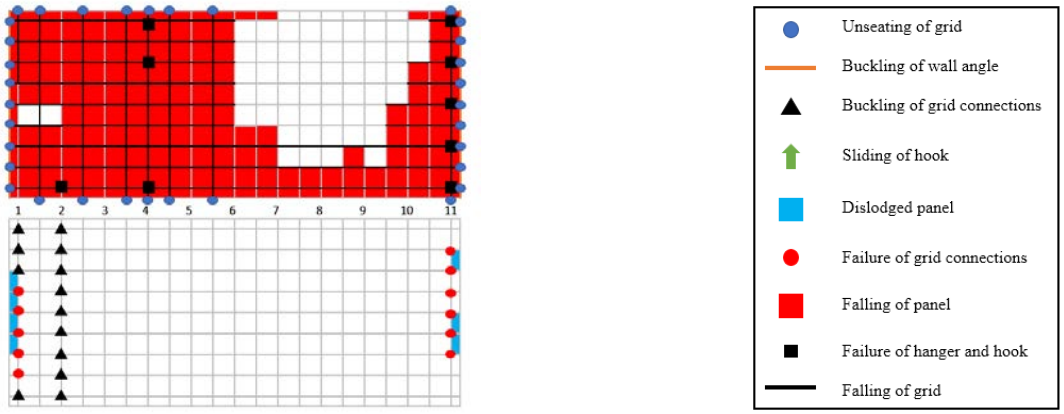

Fig. 6 – Damage to two ceilings after the last run

3.2 Dynamic characteristics

Bi-directional white noises were input to identify the dynamic characteristics of SCSs. However, it was extremely difficult to identify the individual natural frequency of the ceiling system because the excitation intensity and the gap between the ceiling system and the steel platform were so small, which caused the ceiling system to move with the platform together. Therefore, the responses of SCS under the excitation of the sweep wave were used to derive the frequency of the ceiling system by the transfer function method. The natural frequencies of Ceiling A in X and Y directions are approximately 4.0Hz and 3.7Hz, respectively. For Ceiling B, the results in X and Y directions are 2.4Hz and 2.2Hz, respectively. Compared with Ceiling B, the natural frequencies of Ceiling A are greater mainly due to the strong pounding effect between the Ceiling and peripheral beams.

3.3 Acceleration responses

In the current seismic codes of most countries, the equivalent static method is widely recommended for calculating the seismic action of non-structural components, in which the acceleration amplification factor (AAF) is a key parameter representing the location (height) factor [33]. The peak AAF prescribed in Chinese seismic code (GB50011-2010) takes the value of 2.0 for the suspended ceiling system. The AAF is calculated as the ratio of the peak ceiling grid acceleration to the peak floor acceleration.

The axes where D12 to D18 exist are named as Y1 to Y7, respectively. The axes where D19 to D25 exist are named as Y1' to Y7', respectively. The axes where D1 to D11 exist are named as X1 to X11, respectively. The AAF under sweep wave and floor acceleration time history (FATH) excitations are plotted in Figs. 7 and 8, respectively. The observations are obtained from Fig. 7 as follows: (1) the maximum AAF for Ceiling A occurs at the end of the ceiling (except for run 24), whereas the maximum response for Ceiling B is located at the center of the ceiling (Y5') under each input (Fig. 7a), (2) as the intensity of the input from Run 2 to 20 increases, the AAF for Ceiling B gradually increases. However, the AAF decreases from Run 20 to 24 due to the severe damage causing the nonlinear response of Ceiling B (Fig. 7a), (3) Ceiling A produces larger AAF varying from 3.5 to 7.5 caused by the pounding at the boundary, whereas the AAF for Ceiling B is smaller than that of Ceiling A (Fig. 7b), (4) the AAF distribution trend for Ceiling A is not obvious, whereas the maximum response for Ceiling B occurs roughly at the center of the ceiling (X6) under each input (Fig. 7b), and (5) the AAF reduction in Y direction with the aid of the seismic clips is more effective than that in X direction, which is caused by the fact that there are more seismic clips in Y direction and different behavior of the typical ceiling joint allows the slipping in Y direction.

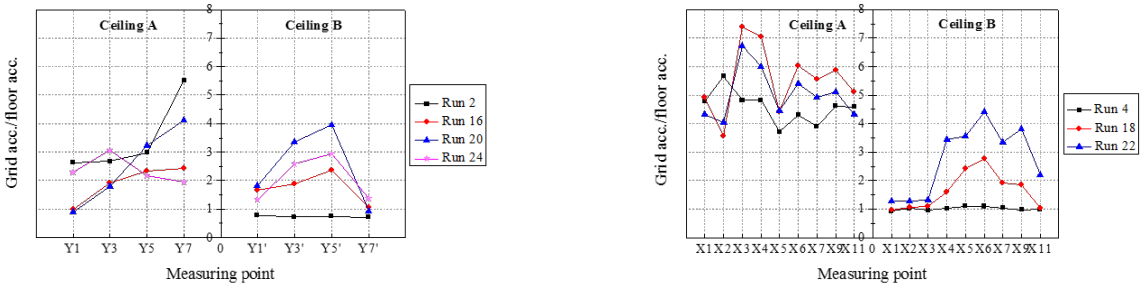

(a) Sweep- input in X direction (b) Sweep- input in Y direction

Fig. 7 – Acceleration amplification factor (AAF) under sweep excitations

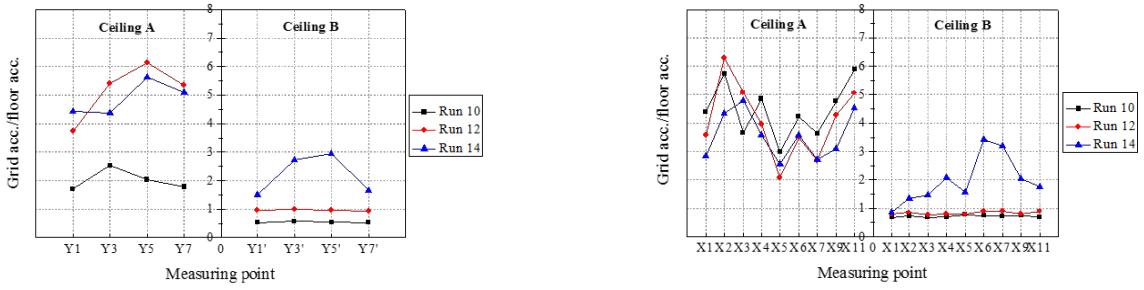

(a) Response in X direction (b) Response in Y direction

Fig. 8 – Acceleration amplification factor (AAF) under FATH excitations

From Fig. 8, it can be founded that (1) whether the responses in X direction or Y direction, the AAF for Ceiling B is much smaller than that of Ceiling A under each excitation, (2) under Runs 12 and 14, the AAF for Ceiling B is even lower than 1.0, (3) for Ceiling A, most of AAFs are greater than 2.0 which is the recommended value in the specifications, which means that the code value needs to be further studied and revised, and (4) the locations of the greatest AAF for Ceiling B in X and Y directions are basically both in the middle of the ceiling on the corresponding direction.

3.4 Displacement responses

The peak displacement (PD) under unidirectional sweep excitations is shown in Fig. 9. From this figure, it can be found that (1) under Run 2 or Run 4, the PD of Ceiling B in X direction, which is close to 0, is much smaller than that of Ceiling A, (2) the PDs of most measuring points of Ceiling B, larger in the middle and smaller on both sides as the result of the constraint effect of the clips in the perpendicular direction, are greater than those obtained from Ceiling A under Runs 16 and 20 (Fig. 9a), (3) under Runs 18 and 22, most of PDs of Ceiling B are smaller than those of Ceiling A (Fig. 9b), (4) compared with the same level of excitation in X direction, most of PDs of these two ceilings in Y direction are smaller because of more seismic clips installed in Y direction, and (5) the sweep wave with higher intensity produces larger PD.

Fig. 10 shows PD of measured points under bidirectional FATH inputs. From this figure, it can be found that (1) under Runs 10 and 12, the PDs of Ceiling B are close to 0, resulting from smaller input intensity and stronger constrains produced by seismic clips, and (2) compared with Ceiling B, the PD of Ceiling A is larger, and PD of D17 point (axis Y6') is larger because of the unseating of the grid end from the wall angle and PD of D3 point (axis X3) is greater due to the buckling of all the ceiling connections on the line.

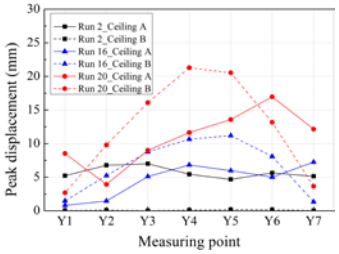

(a) Sweep-X input

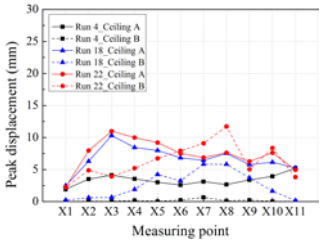

(b) Sweep-Y input

Fig. 9 – Peak displacement under sweep wave

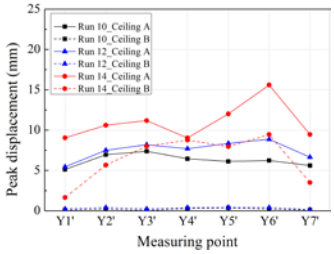

(a) Response in X direction

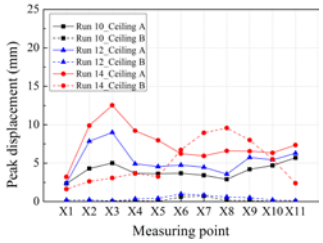

(b) Response in Y direction

Fig. 10 – Peak displacement under FATH inputs

3.5 Strain responses

The maximum strains of ceiling components are shown in Table 3. The maximum strains of all components are much lower than the yield strain of approximately 2000με. However, local buckling was observed in some components due to strong pounding between the ceiling and the boundary board. It should be noted that the strain of 1607με for the threaded rod of Ceiling A was recorded after the last run during which the SCS collapsed while the maximum strain is only 219με under other excitations.

Fig. 11 shows the comparison of strain of typical components for Ceiling A and Ceiling B under sweep waves. Runs 2, 16, 20, and 24 represent the input of the sweep wave in X direction with PGA of 50gal, 150gal, 250gal, and 500gal, respectively. Runs 4, 18, and 22 indicate the sweep wave in Y direction with PGA of 50gal, 150gal, and 250gal, respectively. It can be found that: (1) the strain responses of M8 threaded rod, main tee and carrying channel in Ceiling A are generally larger than that of Ceiling B, (2) the strain

responses of 1200mm-long cross tee and 600mm-long cross tee in Ceiling A are generally greater than that of Ceiling B under the sweep wave input in X direction, however, the strain response of Ceiling A is slightly smaller than those from Ceiling B under the sweep wave input in Y direction, (3) in the case of unidirectional sweep wave input, the strain response of the component increases with the increase of input intensity. Similarly, the strain comparison of Ceiling A and Ceiling B under FATH excitations shows that the strains of all components in Ceiling B are smaller than those in Ceiling A.

Table 3 – The maximum strain of ceiling components

Excitation type	Ceiling type	Maximum strain of ceiling component (με)				
		Threaded rod	Main tee	1200mm-long cross tee	600mm-long cross tee	Carrying channel
Sweep wave	Ceiling A	1607	181	264	137	85
	Ceiling B	278	104	50	29	59
FATH	Ceiling A	254	121	74	107	77
	Ceiling B	201	64	23	21	25

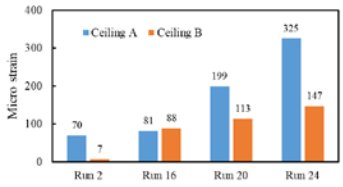

(a) M8 rod under X input

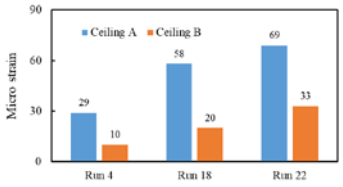

(b) M8 rod under Y input

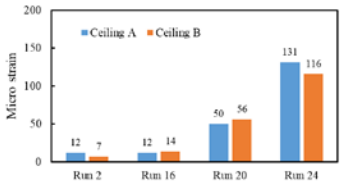

(c) Main tee under X input

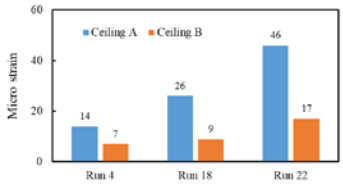

(d) Main tee under Y input

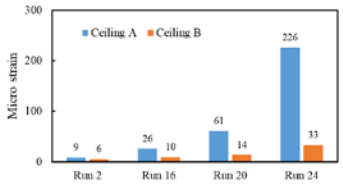

(e) 1200mm-long cross tee under X input

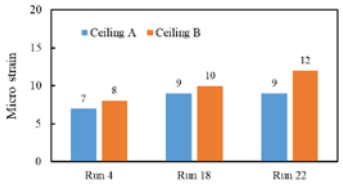

(f) 1200mm-long cross tee under Y input

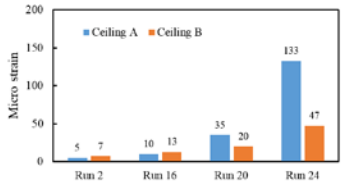

(g) 600mm-long cross tee under X input

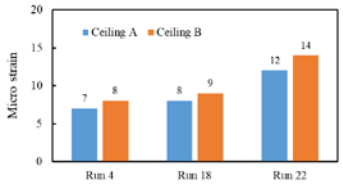

(h) 600mm-long cross tee under Y input

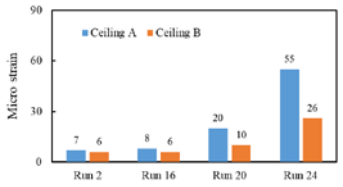

(i) Carrying channel under X input

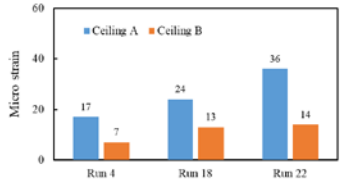

(j) Carrying channel under Y input

Fig. 11 – Strain comparison of Ceiling A and Ceiling B under sweep wave

4. Conclusions

The shaking table tests were carried out on two kinds of full-scale Chinese style SCSs, one without seismic clips and the other with seismic clips. Based on the test results, the following conclusions can be drawn:

1. Ceiling A without seismic clips exhibited damage modes similar to those found in the real earthquake disaster. Compared with Ceiling A, the damage to Ceiling B was much slighter, and the collapse resistance capacity of Ceiling B is improved significantly.

2. The weak axis direction of Chinese style SCSs, which is perpendicular to main tees, is more vulnerable to seismic damage.

3. Compared with Ceiling B, the natural frequencies of Ceiling A are greater, mainly due to the strong pounding between the ceiling and peripheral board.

4. Compared with Ceiling A, in general AAF and PD of Ceiling B are lower. For Ceiling B the AAF and PD in the middle are higher than two sides. In general the strain responses of components in Ceiling B are much smaller than those of Ceiling A.

5. The seismic performance of Chinese style SCSs is significantly affected by the boundary condition. With the installation of seismic clips at the boundary, the seismic performance is improved significantly.

Acknowledgements

The authors acknowledge the financial support from International Joint Research Laboratory of Earthquake Engineering of Tongji University (Grant No.0200121005/058) and International Exchange Program for Graduate Students of Tongji University (Project No.201902017).

References

[1] Dhakal RP, MacRae GA, Hogg K (2011): Performance of ceilings in the February 2011 Christchurch earthquake. *Bulletin of the New Zealand Society for Earthquake Engineering*, **44** (4), 377-387.

[2] Miranda E, Mosqueda G, Retamales R, Pekcan G (2012): Performance of nonstructural components during the 27 February 2010 Chile earthquake. *Earthquake Spectra*, **28** (1_suppl1), 453-471.

[3] Cosenza E, Di Sarno L, Maddaloni G, Magliulo G, Petrone C, Prota A (2015): Shake table tests for the seismic fragility evaluation of hospital rooms. *Earthquake Engineering & Structural Dynamics*, **44** (1), 23-40.

[4] ATC (2015): Performance of buildings and nonstructural components in the 2014 South Napa earthquake. *FEMA P-1024*.

[5] Pourali A (2017): *Seismic performance of suspended ceilings*. University of Canterbury.

[6] Perrone D, Calvi PM, Nascimbene R, Fischer EC, Magliulo G (2019): Seismic performance of non-structural elements during the 2016 Central Italy earthquake. *Bulletin of Earthquake Engineering*, **17** (10), 5655-5677.

[7] Anajafi H (2018): *Improved seismic design of non-structural components (NSCs) and development of innovative control approaches to enhance the seismic performance of buildings and NSCs*. University of New Hampshire.

[8] Devin A, Fanning PJ (2019): Non-structural elements and the dynamic response of buildings: a review. *Engineering Structures*, **187**, 242-250.

[9] Soroushian S, Maragakis EM, Jenkins C (2015): Capacity evaluation of suspended ceiling components, part 1: experimental studies. *Journal of Earthquake Engineering*, **19** (5), 784-804.

[10] Soroushian S, Rahmanishamsi E, Ryu KP, Maragakis M, Reinhorn AM (2016): Experimental fragility analysis of suspension ceiling systems. *Earthquake Spectra*, **32** (2), 881-908.

[11] ANCO (1983): Seismic hazard assessment of nonstructural ceiling components. *NSF Rep. No. CEE-8114155*.

[12] ANCO (1993): Earthquake testing of a suspended ceiling system. *ANCO Engineers*, Culver City, CA.

[13] Riha S, Granneman G (1984): Experimental investigation of the dynamic behavior of building partitions and suspended ceilings during earthquakes. *Rep. No. ARCE R84-1*, California Polytechnic State University, Pomona, CA, USA.

[14] Yao GC (2000): Seismic performance of direct hung suspended ceiling systems. *Journal of Architectural Engineering*, **6** (1), 6-11.

[15] Badillo H, Whittaker AS, Reinhorn AM (2007): Seismic fragility of suspended ceiling systems. *Earthquake Spectra*, **23** (1), 21-40.

[16] Gilani AS, Reinhorn AM, Glasgow B, Lavan O, Miyamoto HK (2010). Earthquake simulator testing and seismic evaluation of suspended ceilings. *Journal of Architectural Engineering*, **16** (2), 63-73.

[17] Soroushian S, Ryan KL, Maragakis M, Wieser J, Sasaki T, Sato E, Alarez D (2012): NEES/E-Defense tests: Seismic performance of ceiling/sprinkler piping nonstructural systems in base isolated and fixed base building. *15th World Conference on Earthquake Engineering*, Lisbon, Portugal.

[18] Pourali A, Dhakal RP, MacRae G, Tasligedik AS (2017): Fully floating suspended ceiling system: experimental evaluation of structural feasibility and challenges. *Earthquake Spectra*, **33** (4), 1627-1654.

[19] Brandolese S, Fiorin L, Scotta R (2019): Seismic demand and capacity assessment of suspended ceiling systems. *Engineering Structures*, **193**, 219-237.

[20] Soroushian S, Rahmanishamsi E, Jenkins C, Maragakis EM (2019): Fragility analysis of suspended ceiling systems in a full-scale experiment. *Journal of Structural Engineering*, **145** (4), 04019005.

[21] Wang D, Dai J, Qu Z, Ning X (2016): Shake table tests of suspended ceilings to simulate the observed damage in the M s 7.0 Lushan earthquake, China. *Earthquake Engineering and Engineering Vibration*, **15** (2), 239-249.

[22] Lu Y, Mosqueda G, Han Q, Zhao Y (2018): Shaking table tests examining seismic response of suspended ceilings attached to large-span spatial structures. *Journal of Structural Engineering*, **144** (9), 04018152.

[23] Kasai K, Mita A, Kitamura H, Matsuda K, Morgan TA, Taylor AW (2013): Performance of seismic protection technologies during the 2011 Tohoku-Oki earthquake. *Earthquake Spectra*, **29** (1_suppl), 265-293.

[24] Masuzawa Y, Kanai T, Hisada Y, Yamashita T, Koizumi S (2017): Study on aseismic performance of integrated ceiling system and anti-fall measures of ceiling. *16th World Conference on Earthquake Engineering*, Santiago, Chile.

[25] J502-2-2012 (2012): *Indoor decoration: suspended ceiling inside*. China Planning Press. (in Chinese)

[26] Federal Emergency Management Agency (2011): Reducing the risks of nonstructural earthquake damage-A practical guide. *FEMA E-74*, Washington DC, USA.

[27] Badillo H, Whittaker AS, Reinhorn AM, Cimellaro GP (2006): Seismic fragility of suspended ceiling systems: *Technical Rep. MCEER-06-0001*, University of Buffalo, Buffalo, NY.

[28] Soroushian S, Maragakis M, Jenkins C (2016): Capacity evaluation of suspended ceiling-perimeter attachments. *Journal of Structural Engineering*, **142** (2), 04015124.

[29] JGJ 339-2015 (2015): *Code for seismic design of non-structural components*. China Architecture and Building Press. (in Chinese)

[30] CECS 255-2009 (2009): *Technical specification for installation of ceiling systems in buildings*. China Planning Press. (in Chinese)

[31] DGJ08-9-2013 (2013): *Code for seismic design of buildings*. (in Chinese)

[32] Lu XL, Jiang C, Jiang HJ (2016): Seismic damage analysis of a benchmark model for Mega-tall buildings. *Journal of Building Structures*, **37** (9): 1-7. (in Chinese)

[33] Lu W, Huang B, Chen S, Mosalam KM (2017): Acceleration demand of the outer−skin curtain wall system of the Shanghai Tower. *The Structural Design of Tall and Special Buildings*, **26** (5), e1341.

